Modeling temporal variations of electrical resistivity associated with pore pressure change in a kilometer-scale natural system

Sophie Hautot

Geochemistry Geophysics Geosystems G3
AN ELECTRONIC JOURNAL OF THE EARTH SCIENCES
Published by AGU and the Geochemical Society

Article
Volume 6, Number 6
15 June 2005
Q06005, doi:10.1029/2004GC000859
ISSN: 1525-2027

Modeling temporal variations of electrical resistivity associated with pore pressure change in a kilometer-scale natural system

Sophie Hautot
School of Geosciences, University of Edinburgh, Edinburgh, UK

Now at IUEM, UMR 6538, CNRS, "Domaines Océaniques," Place Nicolas Copernic, 29280 Plouzané, France (hautot@univ-brest.fr)

[1] From 1995 to 1998 the natural electric field was monitored with an array of 20 dipoles on a ridge separating two reservoir lakes in the French Alps. The experiment was run to study the correlation between the electric potential variations and transient deformations of the ridge in association with the annual cycle of lake level variations. Large distortion of the induced electric field is observed and is found almost purely static and well correlated to the geology. A simple DC 3-D model is constructed, and resistivity structures that create the distortion are identified. The electrically resistive crystalline bedrock strongly amplifies the static distortion caused by the heterogeneous geology on the ridge. The temporal variations of the electric distortion observed over two years are associated with the lake level cycle. The model suggests that a resistivity variation of the order of 20% in the bedrock can account for the observed seasonal time-varying distortion. The resistivity change could be explained in terms of pore and crack geometry change controlled by stress. This study suggests that in particular geological contexts, electrical resistivity changes in structures can be detected through an amplification of the static distortion of the induced electric field. The results provide a framework to interpret some observations of electric field variations possibly associated with tectonic activity. The galvanic coupling model proposed here is an alternative to the streaming potential effect model, and it defines new criteria for the surface detection of groundwater in the crust.

Components: 6154 words, 8 figures.

Keywords: connectivity; magnetotellurics; resistivity; static distortion; strain.

Index Terms: 1515 Geomagnetism and Paleomagnetism: Geomagnetic induction; 5109 Physical Properties of Rocks: Magnetic and electrical properties (0925); 8168 Tectonophysics: Stresses: general.

Received 6 October 2004; **Revised** 7 March 2005; **Accepted** 24 March 2005; **Published** 15 June 2005.

Hautot, S. (2005), Modeling temporal variations of electrical resistivity associated with pore pressure change in a kilometer-scale natural system, *Geochem. Geophys. Geosyst.*, *6*, Q06005, doi:10.1029/2004GC000859.

1. Introduction

[2] The electrical resistivity of a rock is very sensitive to its fluid content. Recently, a percolation model has been proposed to explain the telluric distortion observed in magnetotelluric (MT) data [*Bahr*, 2000; *Bahr et al.*, 2002], introducing the important role of fluids in the distortion of the induced electric fields. Electromagnetic methods could provide a valuable tool for fluid characterization if one could detect small time changes in the electrical resistivity of underground structures. This is important for hydrogeological problems but also in active tectonics where fluids are known to play an important role in the seismic cycle [*Nur and Booker*, 1972; *Muir-Wood and*

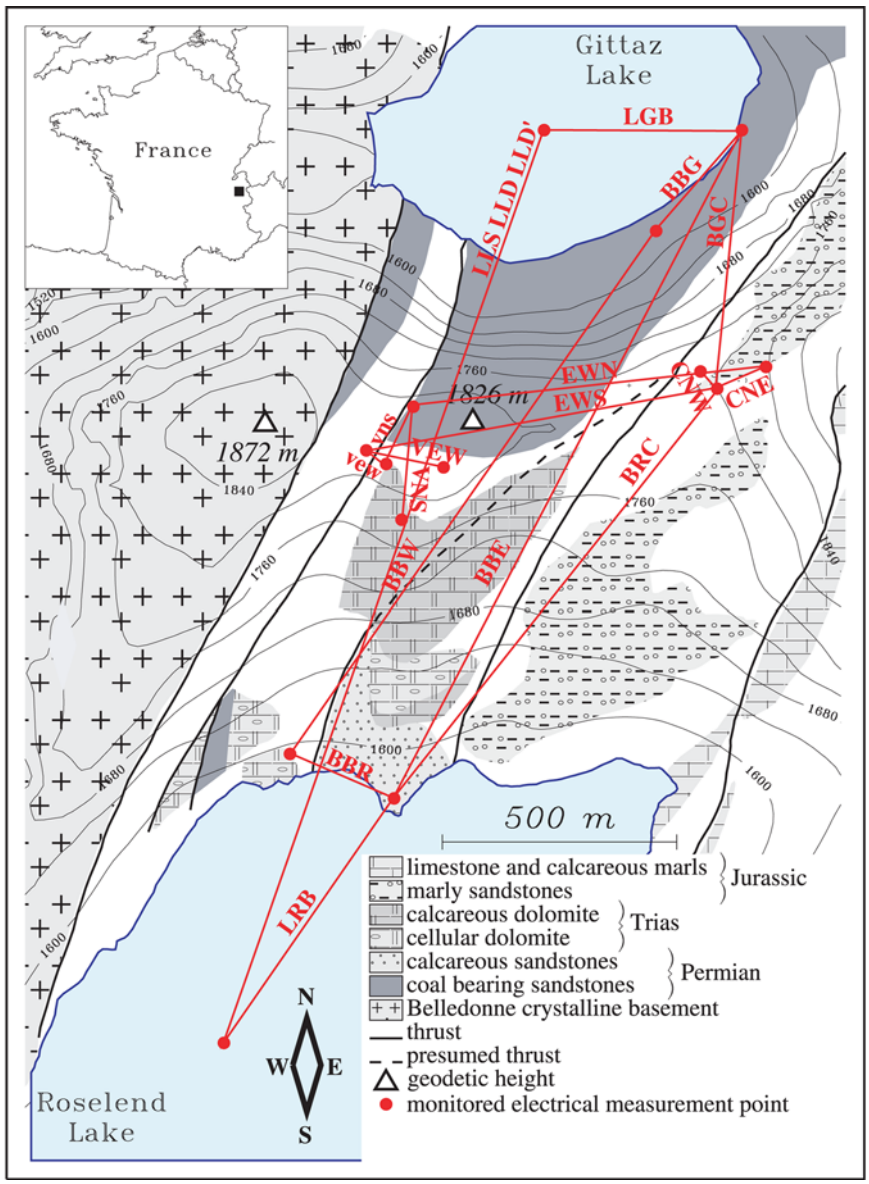

Figure 1. Geological map of the Sur-Frêtes area, showing the location of the electrical measurement points and the dipole array.

King, 1993; *Miller et al.*, 1999]. Continuous electrical monitoring in active areas might therefore provide some clues to the understanding of the relationship between subsurface fluids and seismic activity. Such experiments already exist and changes in conductivity have been associated with mechanical stress [*Park and Fitterman*, 1990; *Park et al.*, 1993; *Chu et al.*, 1996]. Nevertheless, the simple physical models proposed to reproduce field observations resulted in unrealistically high strain [*Quian*, 1985; *Madden et al.*, 1993].

[3] The Sur-Frêtes ridge, located in the French Alps, is a kilometer-scale laboratory for the study of the physical phenomena associated with the deformation of a natural system under controlled mechanical and hydrological solicitation [*Trique et al.*, 2002]. The ridge separates two artificial lakes (Figure 1) whose water levels vary on a yearly cycle, inducing changing mechanical stress on the ridge. An array of 14 electrical measurement points was set across the Sur-Frêtes ridge, and the electrical potential differences were measured at 20 dipoles (Figure 1). Additionally, the three components of the magnetic field were recorded with a fluxgate magnetometer installed on the top of the ridge. The electrical and magnetic data were measured almost continuously from November 1995 to

December 1998. Variations of the induced electric field associated with the lake level variations have been observed, for some amplitude ratios between electric dipoles [*Trique et al.*, 2002].

[4] In this paper, I propose that these temporal variations are related to change in bulk resistivity of two-phase system in the basement. The effect of the resistivity change is observable because the static distortion of the electric field is strongly amplified by the galvanic coupling between the shallow structures and the crystalline basement. A simple resistivity model can explain the distortion measured with the electric array. It is found that the variation of one single parameter of the model can account for the temporal variations of the telluric distortion associated with the lake levels annual cycle. A physical model is proposed to explain the resistivity change observed in terms of pore connectivity variation associated with the pressure change induced by the lakes loading.

2. Magnetotelluric Data

[5] The whole period electric and magnetic time series recorded during the Sur-Frêtes experiment (the sampling rate is 1 minute) have been used to calculate the MT response function for all but one dipole (that excluded had too many interruptions in the time series). Because of cable damage from March to October 1996 resulting in the loss of data, only data acquired from October 1996 to December 1998 are considered in this study. MT response functions were obtained, relating the electric field (E) to the magnetic field (B) in the frequency domain. The MT response function is usually presented as an impedance tensor:

$$\begin{pmatrix} E_x \\ E_y \end{pmatrix} = \begin{pmatrix} Z_{xx} & Z_{xy} \\ Z_{yx} & Z_{yy} \end{pmatrix} \begin{pmatrix} B_x \\ B_y \end{pmatrix}, \quad (1)$$

where x and y are the north and east directions, respectively. Here, due to the experiment design (Figure 1), we have instead a total of 19 response functions, relating the electric field for a given dipole (E_θ, with θ being the dipole direction measured clockwise from North) to the magnetic field (B) in the frequency domain.

$$E_\theta = Z_{\theta 1} B_x + Z_{\theta 2} B_y. \quad (2)$$

[6] The response functions $\mathbf{Z}_\theta$($Z_{\theta 1}$ and $Z_{\theta 2}$) were computed using robust remote reference processing [*Chave and Thomson*, 1989] in period range 870 s to 40 hours. The magnetic remote reference was the geomagnetic observatory of Chambon-la-Forêt (France).

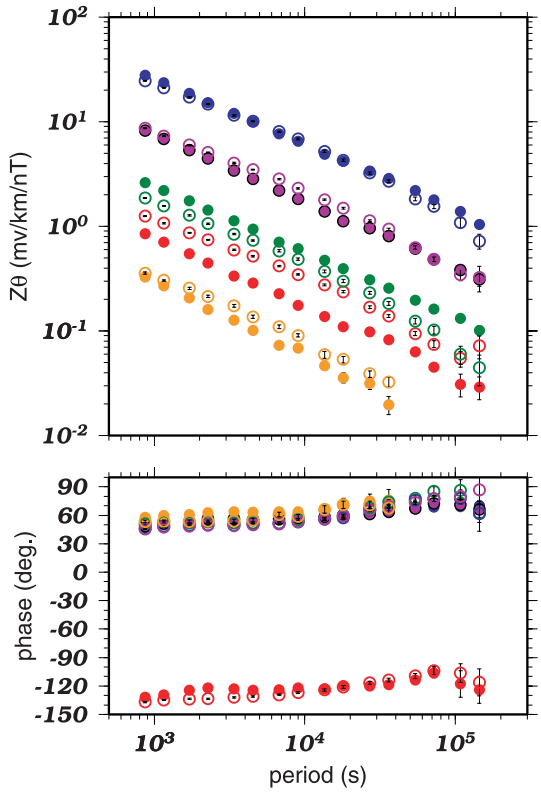

Figure 2. Amplitude and phase of $Z_\theta 1$ (open symbols) and $Z_{\theta 2}$ (solid symbols) for 5 of the dipoles. Red, BBE; green, BRC; blue, CNE; purple, EWS; orange, BBW (Figure 1).

[7] A strong distortion of the electric field is observed on all the dipoles, and over the whole period range. As an illustration, five of the 19 response functions are shown in Figure 2. The offset between the impedance amplitude curves at each dipole, independent of period, coupled with no phase difference between the response functions (Figure 2) is typical of the so-called static shift [*Jones*, 1988]. The static (DC) distortion is due to the presence of electric charges on heterogeneities at shallow depths (< skin depth). As a result, the effect of galvanic currents is added to the induction response. We observe a strong DC distortion of the electrical fields regardless of dipole length (51–2052 m), direction (6–136°N), and electrode position. Therefore very local galvanic effects due to heterogeneity in the vicinity of the electrodes, which can often be the source of static shift [*Jones*, 1988; *Perrier et al.*, 1997], do not seem to control

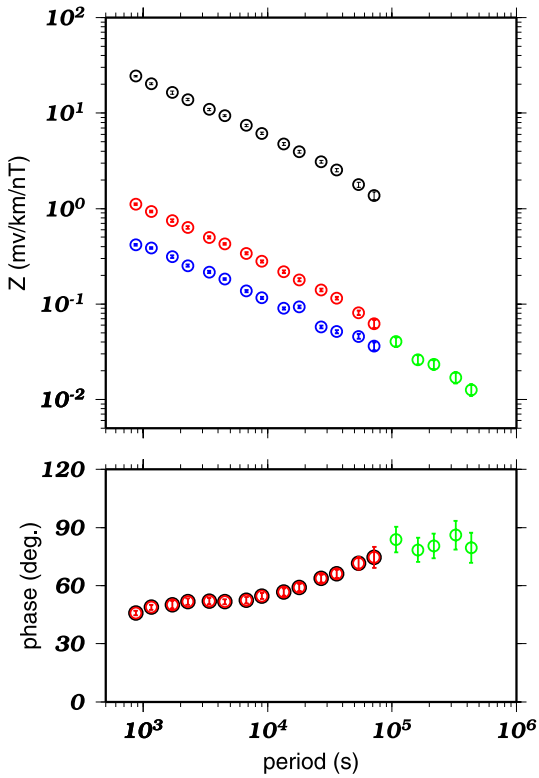

Figure 3. Amplitude and phase of the MT transfer function. Z_1 (black) and Z_2 (blue) are the maximum and minimum values of the MTI tensor. Red circles are the static shift corrected **Z**. Green circles are the response function Z_m obtained from the geomagnetic deep sounding data. The normal response function Z_n was obtained by combining **Z** (870–72,000 s) and Z_m (108,000–432,000 s).

the large electric field distortion observed in the Sur-Frêtes ridge data.

[8] A mean MT impedance (MTI) tensor **Z**, representative of the Sur-Frêtes ridge, was obtained from the analysis of the $\mathbf{Z}_\theta$ variation with the θ direction (periods from 870–72,000 s). The values $Z_{\theta x}$ and $Z_{\theta y}$ are a linear combination of the four MTI coefficients Z_{xx}, Z_{xy}, Z_{yx}, Z_{yy}, cos θ and sin θ. Solving the system $(Z_{\theta_i}x, Z_{\theta_i}y) = F_i(Z_{xx}, Z_{xy}, Z_{yx}, Z_{yy})$ with i = 1 to 19 gives the four MTI coefficients. The direction of maximum (Z_1) and minimum (Z_2) values of MTI were obtained from the tensor decomposition approach proposed by *Counil et al.* [1986] (Figure 3). The calculated impedance tensor **Z** was corrected for static shift using the geomagnetic deep sounding data (from which a response function Z_m between the vertical Z and the north geomagnetic H components was calculated) at the longest periods (40,500–432,000 s). At these periods T, the external source field is uniform [*Banks*, 1969] and Z_m is related to Z and H by

$$Z_m = -\frac{1}{2} i\omega\mu_0 a \frac{Z}{H} \tan\phi, \tag{3}$$

where $\omega = 2\pi/T$, μ_0 is the magnetic permeability, a is the Earth radius (6371 km), and ϕ is the colatitude. A normal impedance response function Z_n was obtained, appropriate for a 1-D Earth [*Tarits et al.*, 2004] (Figure 3).

3. Electric Field Distortion Parameter

[9] The response function $\mathbf{Z}_\theta$ at a given period (9000 s) is shown versus θ in Figure 4. The amplitude of $\mathbf{Z}_\theta$ varies with dipole orientation, whereas its phase is constant. We observe a minimum in the amplitude at about 35°N. This direction corresponds to the regional tectonic trend (Figure 1). The relationship between $\mathbf{Z}_\theta$ and θ suggests that the scale of the distortion is of the order or larger than the electric array (i.e., ≥ kilometer scale), and we may assume that a common source, perhaps associated with the geology, accounts for the observed distortion. This hypothesis may be tested because we can characterize quantitatively the electric field distortion measured with a telluric array.

[10] Let us consider the distortion tensor **T**. The tensor **T** has four real elements (which are

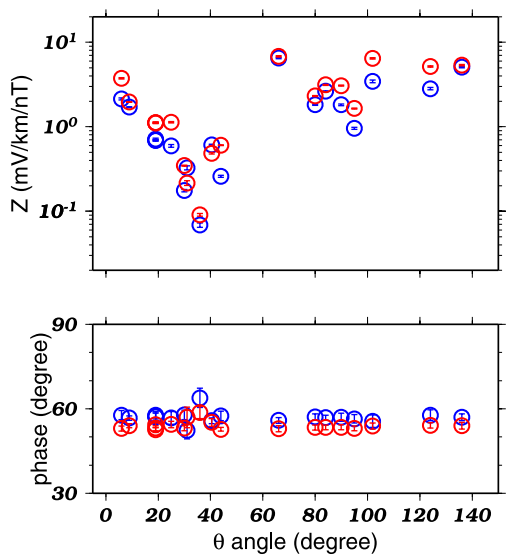

Figure 4. Amplitude and phase of $Z_\theta 1$ (blue symbols) and $Z_{\theta 2}$ (red symbols) as a function of θ (dipole direction measured clockwise from north) and at a period of 9000 s.

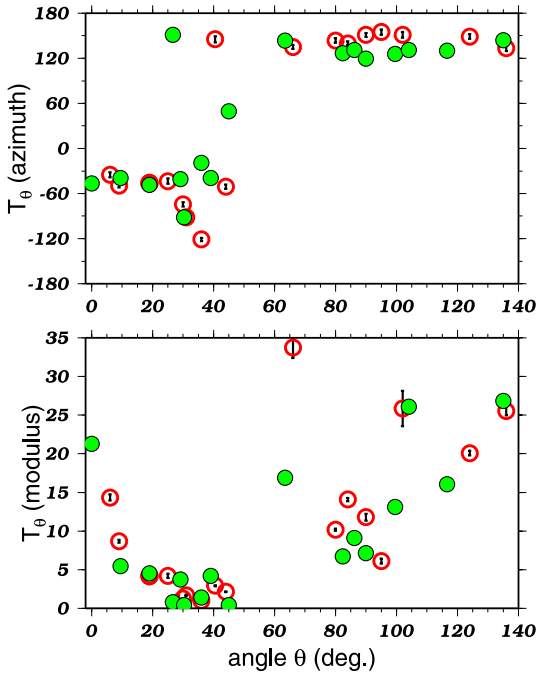

Figure 5. (bottom) Modulus and (top) azimuth of the real vector T_θ as a function of θ. Red circles are calculated from the data. Green dots are predictions of the model shown in Figure 6.

frequency independent in our data frequency range) and relates the measured electrical field **E** to the normal electrical field $\mathbf{E_n}$, that would be measured in the absence of any perturbation [*Larsen*, 1975; *Le Mouël and Menvielle*, 1982]. Here, the normal field is for a regional 1-D conductivity medium [*Tarits et al.*, 2004].

$$\mathbf{E} = \mathbf{E_n} + \mathbf{T}\mathbf{E_n}. \tag{4}$$

Given that in the frequency domain,

$$\mathbf{E_n} = \mathbf{Z_n}\mathbf{B_n}, \tag{5}$$

where $\mathbf{B_n}$ is the regional normal magnetic field, equation (1) is equivalent to

$$\begin{pmatrix} E_x \\ E_y \end{pmatrix} = Z_n \begin{pmatrix} -T_{xy} & 1+T_{xx} \\ -(1+T_{yy}) & T_{yx} \end{pmatrix} \begin{pmatrix} B_{nx} \\ B_{ny} \end{pmatrix}. \tag{6}$$

Therefore we have

$$\begin{aligned} E_x &= Z_n\left(-T_{xy}B_{nx} + (1+T_{xx})B_{ny}\right) \\ E_y &= Z_n\left(-(1+T_{yy})B_{nx} + T_{yx}B_{ny}\right), \end{aligned} \tag{7}$$

and the electric field measured at each dipole is

$$E_\theta = \cos\theta E_x + \sin\theta E_y. \tag{8}$$

If we define the parameters $T_{x\theta}$ and $T_{y\theta}$ by

$$\begin{aligned} T_{x\theta} &= \cos\theta T_{xx} + \sin\theta T_{yx} \\ T_{y\theta} &= \cos\theta T_{xy} + \sin\theta T_{yy}, \end{aligned} \tag{9}$$

then equations (5) and (6) give

$$E_\theta = Z_n\left(-(\sin\theta + T_{y\theta})B_{nx} + (\cos\theta + T_{x\theta})B_{ny}\right), \tag{10}$$

and equations (1) and (8) give

$$\begin{aligned} Z_{\theta 1} &= Z_n\left(-(\sin\theta + T_{y\theta})\right) \\ Z_{\theta 2} &= Z_n(\cos\theta + T_{x\theta}). \end{aligned} \tag{11}$$

The vector $\mathbf{T}_\theta$ (with the two components $T_{x\theta}$ and $T_{y\theta}$; equation (9)) is real and characterizes the distortion in the θ direction. The calculated $\mathbf{T}_\theta$ for each dipole are shown in Figure 5, in terms of modulus and azimuth, as a function of θ. Again, a relationship with the θ direction is observed, with a 90° variation of the azimuth angle and a minimum of the vector modulus at $30° < \theta < 45°$, which corresponds to the tectonic trend (within this angle range, the modulus of $\mathbf{T}_\theta$ is very small, which explains the discrepancy of the $\mathbf{T}_\theta$ azimuth angle).

4. Modeling

4.1. Resistivity Model

[11] In the classical application of MT to regional studies, the source of the static distortion of the electromagnetic field is local compared to the scale of the investigated structures. The static distortion is generally considered as noise and the tensor decomposition is the most commonly used method to separate the galvanic effects from the inductive response [*Bahr*, 1988; *Groom and Bailey*, 1989]. With this technique, no physical interpretation of the galvanic current source is possible. In this study we established that the electric field distortion source is at least at the kilometer-scale and that it could be associated with the geology. However, this is not sufficient to describe the static distortion we observed and to interpret it in terms of physical properties of the Sur-Frêtes ridge system. Therefore numerical modeling is proposed to attempt to identify the location and shape of the source of the static electric field distortion.

[12] The static distortion of MT data is due to the accumulation of electric charges along a resistivity contrast at shallow depth. The geology of the Sur-Frêtes ridge is heterogeneous and resistivity variations may be expected between the different geological structures that were identified in the area (Figure 1). This was confirmed by electromagnetic surveys that were carried out on the ridge. Results show large resistivity contrast, locally more than three orders of magnitude, along an east-west profile on the top of the ridge [*Hautot et al.*, 2002]. Therefore, given our knowledge of the geology, it is possible to consider resistivity models that reproduce the telluric distortion observed on the MT data.

[13] Since the static shift is purely galvanic, the DC principles apply to simulations of MT conditions [*Spitzer*, 2001]. Let us consider a single source of current at a distance tending toward infinity from the potential measurements points. In the presence of a heterogeneity aligned in the θ direction, the electric field measured with the dipole is

$$E_\theta = E_{n\theta} + \mathbf{T}_\theta \mathbf{E_n}, \tag{12}$$

where $E_{n\theta}$ is the normal electric field in the θ direction that would be measured in the absence of the heterogeneity. If the current source is in the y direction, the electric field in the x direction is ≈0, thus equation (10) becomes

$$E_\theta = \sin\theta E_{ny} + T_{y\theta} E_{ny}. \tag{13}$$

Therefore, for one dipole in the θ direction, it is only necessary to calculate the normal electric field and the total electric field to obtain the parameter $T_{y\theta}$:

$$T_{y\theta} = \frac{E_\theta}{E_{ny}} - \sin\theta. \tag{14}$$

Respectively, if the current source is in the x direction, we have

$$T_{x\theta} = \frac{E_\theta}{E_{nx}} - \cos\theta. \tag{15}$$

Equations (14) and (15) give the modeled electric field vector distortion parameter $\mathbf{T}_\theta$, which is comparable with the vector $\mathbf{T}_\theta$ derived from the MT data.

[14] In order to validate the hypothesis that the electric distortion observed at Sur-Frêtes has a single and large-scale origin (> dipole length), only simple structures were considered. I used a 3-D code [*Spitzer*, 1995] to calculate the DC response of resistivity structures. For numerical reasons, the grid used for the model was limited to a 50 × 50 meter mesh size. As a result, the electrode positions and the dipole orientations could not be reproduced precisely.

[15] The initial model was based on the results from very-low-frequency and audiomagnetotelluric soundings carried out along an east-west profile on the top of the Sur-Frêtes ridge. A 2-D resistivity model was obtained from the MT data analysis [*Hautot et al.*, 2002] showing a vertical resistivity contrast between a conductive medium to the west and a resistive medium to the east. The model takes into account the rugged topography [*Hautot et al.*, 2002]. The vertical contact was interpreted as the contact between the coal-bearing sandstone and the limestone/dolomite formation (Figure 1). Several trials were made before achieving the structure shown in Figure 6. For each trial, the electric field distribution that was calculated at the surface of each model allows the parameter $\mathbf{T}_\theta$ to be calculated for each dipole of the electric array. The calculated and observed values were compared. The normal electric field at the surface of the model was determined for a layered Earth, and the total electric field was determined by adding a large-scale heterogeneity to the 1-D structure. Several parameters have been considered for the trial-and-error modeling of the observed static distortion parameter, including (1) the resistivity and thickness of the horizontal layers and (2) the resistivity and shape of the large-scale heterogeneity.

[16] The location and shape of a heterogeneity that allows the reproduction of the variations of the observed $\mathbf{T}_\theta$ with θ were successfully obtained after several tests. However, it became rapidly clear that the amplitude of the telluric distortion observed on the Sur-Frêtes ridge could not be reproduced with the modeling of superficial heterogeneity only. The calculated $\mathbf{T}_\theta$ remain very small (modulus <1 for all dipoles) in comparison with the observed values. A natural amplifier of the electric field distortion had to be considered. One source of amplification of the telluric field is the galvanic coupling between two conductive media when they are separated by a highly resistive medium [*Ranganayaki and Madden*, 1980]. In particular, galvanic distortion of crustal origin can affect long-period MT data, and thus their interpretation in terms of the Earth's mantle conductiv-

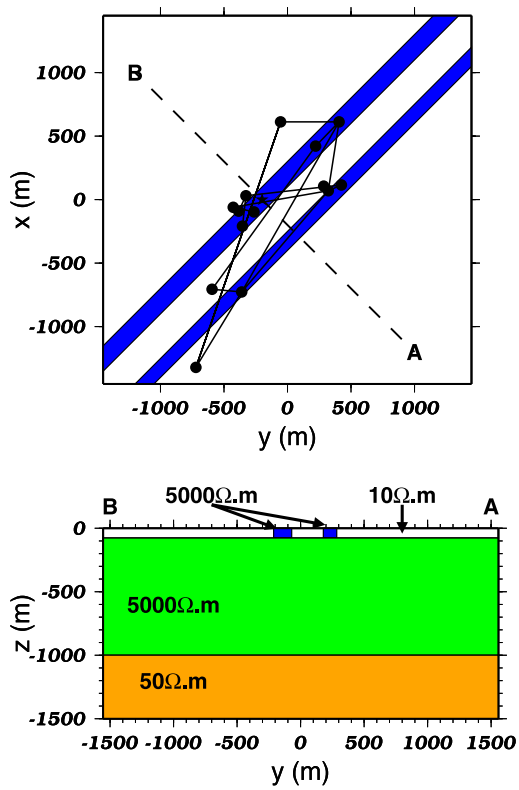

Figure 6. DC resistivity model. The best-fitting three-dimensional resistivity model, with two elongated structures within a layered Earth, includes a resistive layer between 75 and 1000 m depth. (top) Plan view. (bottom) Vertical cross section. Resistivity: white, 10 Ω.m; blue, 5000 Ω.m; green, 5000 Ω.m; orange, 50 Ω.m. Black dots are the electrodes.

ity [*Menvielle and Tarits*, 1994]. In this context, galvanic distortion can be particularly strong when the lower crust is very resistive [*Madden et al.*, 1993; *Tournerie and Chouteau*, 2002], and for seafloor MT data because of the very conductive ocean [*White et al.*, 1997; *Nolasco et al.*, 1998].

[17] The galvanic coupling depends on the resistivity structure and may be observed at all scales. In the Sur-Frêtes model, the galvanic distortion amplification by an intermediate resistor between two conductive layers was considered (Figure 6). For some of the dipoles this situation provided amplification by a factor >30 of the magnitude of the $\mathbf{T}_\theta$ values that were calculated when considering a heterogeneous layer above a conductive half-space. The best-fitting model (Figure 6) was obtained when two thin SW-NE elongated resistors in a conductive layer (75 meters thick, $\rho = 10$ Ω.m) were considered. Given the crude gridding, the two resistors ($\rho = 5000$ Ω.m) can be estimated to be 120–160 and 90–130 m wide, respectively, and separated by 230–270 m. The conductive layer overlies a resistive layer (925 m thick, $\rho = 5000$ Ω.m), which in turn overlies a half-space ($\rho = 50$ Ω.m).

[18] $\mathbf{T}_\theta$ predicted by the best-fitting model is shown for each dipole in Figure 5, with the observed values for comparison. The fit is reasonable although the θ direction was not correctly reproduced by the model for each dipole. The $\mathbf{T}_\theta$ variation with respect to the θ direction shows a minimum in the modulus and a 90° increase in the azimuth for $25° \leq \theta \leq 45°$. For two dipoles ($\theta = 66°$ and 102°N) the observed values of the $\mathbf{T}_\theta$ modulus are larger than the general trend. This behaviour is reproduced in the model.

[19] The fit between the data and the model response is controlled by a few features of the model. (1) The conductive-over-resistive layer configuration is required to reproduce the respective signs of $T_{x\theta}$ and $T_{y\theta}$. (2) The direction of the heterogeneity controls the modulus minimum and the azimuth variation at $\theta \approx 25–45°$. (3) For each dipole, the modulus of T_θ is constrained by the width and the location of the resistors (two resistors instead of one single and large resistor are required), by the resistivity contrast between the heterogeneity and the host layer, and most importantly by the resistivity contrast between the conductive layer and the underlying resistive layer. In contrast, the thickness of the layers has a smaller effect on variation of $\mathbf{T}_\theta$.

4.2. Interpretation

[20] The model shown in Figure 6 has a simple resistivity structure. Nevertheless, it allows most of the electric field distortion observed at the Sur-Frêtes ridge to be simulated. This suggests that the source of the distortion is homogeneous at the site scale, since only two narrow 2-D resistors are sufficient to account for most of the $\mathbf{T}_\theta$ observed. Dipoles oriented along the heterogeneity axis are relatively unaffected by distortion, since it is the off-strike electric field that is distorted by resistivity contrasts. The source of the distortion is related to the regional geology even though the main contribution is from superficial origin (the heterogeneous layer is 75 m thick).

[21] The Sur-Frêtes ridge is at a major geological contact between the Belledonne crystalline basement to the west and Permian-Triassic tectonized sedimentary units to the east, over-thrust by Jurassic calcareous sheets (Figure 1). The

Permo-Triassic units dip about 50°E and are highly heterogeneous. Groundwater flow was associated with the conductive structures observed in the MT model [*Hautot et al.*, 2002]. The two elongated superficial resistors could correspond to fresh rocks units (resistive) embedded in fractured zones (conductive). The western limit of both resistors (Figure 6) corresponds to two thrusts observed in the field (Figure 1), both affecting the coal-bearing sandstone. The very low resistivity deduced for the uppermost layer of the model (ρ = 10 Ω.m) is not unrealistic. Indeed, the apparent resistivity determined from Schlumberger DC measurements performed along the southern bank of La Gittaz lake, along the coal-bearing sandstone outcrop was locally lower than 3 Ω.m [*Trique et al.*, 2002]. The origin of these small values could be graphite layers embedded in the coal-bearing sandstone. The galvanic distortion caused by the presence of those two resistivity contrasts along fractures zones may be largely amplified at the Sur-Frêtes ridge because the sedimentary units lay uncomformably on the highly resistive crystalline bedrock (Belledonne basement).

5. Temporal Variations

[22] At the Sur-Frêtes ridge, temporal variations of the static distortion associated with the yearly lake level cycles were evidenced by calculating electric field amplitude variations ratio between two dipoles. These ratio are free of geomagnetic fluctuation suggesting a local source effect for the temporal variations observed [*Trique et al.*, 2002]. The observations suggest changes in the resistivity structure. Here, the parameterization of the telluric distortion is used to quantitatively investigate the possible resistivity change. The telluric distortion parameter $\mathbf{T}_\theta$ shown in Figure 5 was calculated over the whole duration of the experiment. Now, in order to characterize the temporal variations of the static distortion for each dipole independently, the vector $\mathbf{T}_\theta$ has been calculated with a 4 day time-span between October 1996 and December 1998. To avoid instability problems of $\mathbf{T}_\theta$ obtained from such short time series, equation (2) was used in the time domain since $\mathbf{T}_\theta$ is real. $\mathbf{E_n}(t)$ was generated from Z_n (Figure 3) and the magnetic data after inverse Fourier transform of equation (3). Within each four day period, a robust procedure was used to solve equation (2), the unknown parameter being $\mathbf{T}_\theta$, where θ is the electric field direction. The calculation has been made for all the dipoles.

[23] Results are shown in Figure 7 together with the Roselend and La Gittaz lake level variations [*Trique et al.*, 2002]. The amplitude of the temporal variations of $\mathbf{T}_\theta$ is above the noise level, as shown by its comparison with the error bars in Figure 5. There is a clear relationship between the induced electric field distortion and the lake level variations. The correlation coefficient between $\mathbf{T}_\theta$ and the lake levels varies from 0.7 to 0.96. Results are shown for 3 representative dipoles (LGB, VEW, and BBW; see Figure 1). Dipoles LGB and VEW are shown because they show similar large-amplitude and contemporaneous variations although one of the electrodes of LGB is in lake La Gittaz whereas VEW is on the top of the ridge. The two dipoles have similar orientations, roughly perpendicular to the strike (90° and 102°N). Dipole BBW is representative of the dipoles with an orientation near the strike. Even though the modulus of $\mathbf{T}_\theta$ is small for these dipoles, the azimuth angle shows large-amplitude variations, again correlated with the lake level variations.

[24] The maximum amplitude of temporal variations of $\mathbf{T}_\theta$ are shown versus θ in Figure 8 for each dipole. The maximum deviation presented corresponds to the difference between $\mathbf{T}_{\theta\mathbf{max}}$ and $\mathbf{T}_{\theta\mathbf{min}}$, the highest (when the lake levels are low) and lowest (high lake levels) values of the $\mathbf{T}_\theta$ time series, respectively. There is some uncertainty in the calculated values, particularly for the small $\mathbf{T}_\theta$ values when high frequency variations are added to the yearly cycle. This introduces some dispersion in the results shown in Figure 8. Dipole vns (θ = 25°) has been discarded because the time series are too short to determine whether there is an annual variation in the static distortion of the electric field measured with this dipole.

[25] The real vector $\mathbf{T}_\theta$ is a static shift factor of the induced electric field (equation (4)). Therefore temporal variations of $\mathbf{T}_\theta$ should be related to changes in the resistivity structure of the underground medium. This may be tested by varying the resistivity of the structures in the model. We have seen that both the resistivity contrast in the superficial layer and the resistivity contrast between the uppermost layer and the resistive layer underneath control the magnitude of the parameter $\mathbf{T}_\theta$. Thus I observed the change in the static distortion when I varied (1) the resistivity value in the superficial layer (initially ρ_1 = 10 Ω.m, the resistivity in the rest of the model is kept constant) and (2) the resistivity value in the resistive layer (initially ρ_2 = 5000 Ω.m). The two different tests

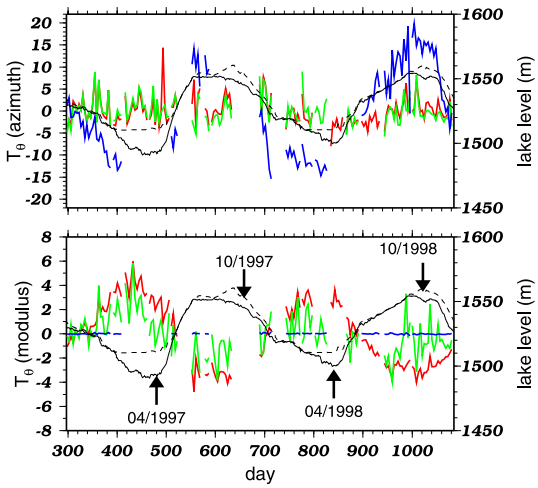

Figure 7. Observed real vector $\mathbf{T}_\theta$, (bottom) modulus and (top) azimuth versus time (day 297 = 23/10/1996) for 3 dipoles, LGB (red), VEW (green), and BBW (blue). Thin lines are for the Roselend (solid line) and La Gittaz (dashed line) lake levels. The average of modulus and azimuth have been removed for the dipole comparisons.

give similar results when ρ_1 is decreased by 50% or when ρ_2 is varied by ±10%. The results for the latter case are shown in Figure 8. The calculated distortion variations agree to some extent with the observed values. Some large distortion variations could not be reproduced, as for $\theta = 90°$, this may be due to the simplicity of the resistivity model.

[26] The two tests performed with the model indicate two possible sources for the variation of the telluric distortion, a resistivity change can occur in either the uppermost conductive layer or the underlying resistive layer. One argument suggests that the resistivity changes in the resistive layer: The model shown in Figure 6 allows to simulate the time average value (TAV) of the static distortion of the telluric field calculated with the complete time series (Figure 5). The mean value of the observed $\mathbf{T}_\theta$ calculated for all the four days $\mathbf{T}_\theta$ samples is similar to the TAV since two complete cycles have been measured during the experiment (Figure 7). Thus the mean value is not biased. Therefore, when considering the modeling, one may expect to reproduce the temporal variations observed when varying the resistivity of the medium above and below the value obtained for the $\mathbf{T}_\theta$ mean value. This is the case with the resistive layer when ρ_2 is set to ±10% of the average value. In contrast, increasing or decreasing ρ_1 from the average value results indifferently in a decreasing of the $\mathbf{T}_\theta$ modulus.

[27] These results show that resistivity change in the underground structure can account for the temporal variation of the telluric distortion observed on the Sur-Frêtes ridge. The modeling indicates that the modulus of $\mathbf{T}_\theta$ increases with resistivity. That is, when the lake levels decrease, resistivity in the underground structures increases (Figure 7). There is no apparent significant time lag between the lake level variations and the response of the system (Figure 7) suggesting that the resistivity in the crystalline basement (ρ_2) varies almost simultaneously with the lake levels.

[28] Resistivity change associated with mechanical stress were first observed in laboratory experiments some years ago and have been found to be related to crack closure and opening under stress [e.g., *Walsh and Brace*, 1984]. The resistivity variation at Sur-Frêtes could reasonably be interpreted as the response of the ridge to the mechanical stress induced by the lake level variations. The yearly stress variations of the Sur-Frêtes ridge were estimated to be of the order of 10^4 Pa [*Perrier et al.*, 1998]. From the modeling results, the change of resistivity with pressure would be of order 20% in

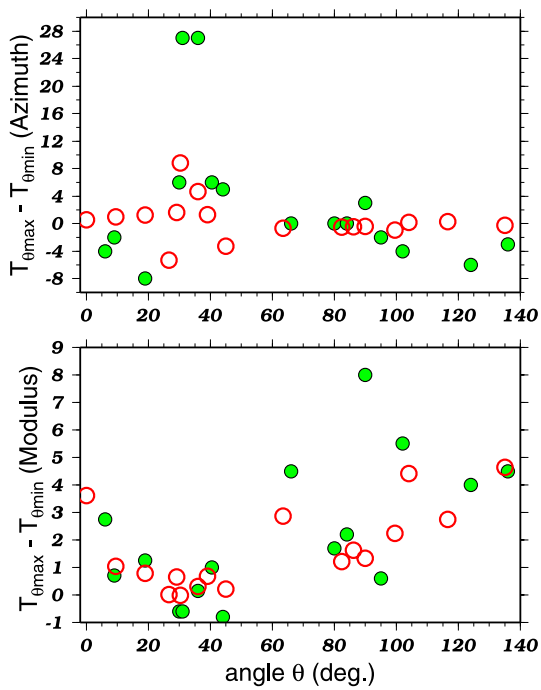

Figure 8. Maximum deviation of the (bottom) modulus and (top) azimuth of real vector T_θ as a function of θ. Green symbols are observed values. Red circles are predicted by the model. The predicted values correspond to the difference between the calculated T_θ when the resistivity of the resistive layer is changed from 5500 Ω.m to 4500 Ω.m.

bedrock resistivity. These results are comparable with laboratory experiments on low-porosity crystalline rocks, where an increase in resistivity of up to 50% was observed for a 5 MPa pressure increase [*Brace et al.*, 1965]. However, even considering a small porosity for the crystalline basement of 1% and using the Archie's law, the yearly resistivity change of 20% would require a strain of 10^{-3}. This volume change is far too large considering the $10^{-7} day^{-1}$ strain rate estimated for the ridge [*Trique et al.*, 1999]. If the resistivity change is interpreted in terms of pore volume change, our results would lead to the same conclusion as those from previous studies in tectonically active areas where observed resistivity change were found to imply unrealistically high strain [*Quian*, 1985; *Madden et al.*, 1993].

[29] The pore geometry redistribution model requires less strain to explain resistivity change. This model was previously suggested to explain resistivity change prior to earthquakes [*Merzer and Klemperer*, 1997]. Laboratory experiments on water saturated sandstones in the undrained regime (the fluid volume was kept constant) have shown that the resistivity of the samples were particularly sensitive to the connectivity of the crack network [*Glover et al.*, 2000]. *Hautot and Tarits* [2002] have shown that it is possible to detect such resistivity change with surface measurements. They calculated the resistivity of fluid-saturated porous structures at the field scale using 3-D models of random porosity. They defined a parameter that characterizes the connected fraction of the fluid phase and they showed that this parameter controls the electrical properties of the heterogeneous media. It was observed that for porosity <10%, the resistivity is very sensitive to the geometry of the connected pores network. A maximum of 40% resistivity difference was obtained for heterogeneous media with a constant fluid volume but a different random pore geometry, hence a different connectivity parameter [*Hautot and Tarits*, 2002]. Those results suggest that minor strain of the Sur-Frêtes ridge should be sufficient to generate significant variation of the low-porosity crystalline bedrock resistivity.

6. Implications and Conclusions

[30] This paper presents the analysis of kilometer-scale telluric distortion observed in a system under controlled mechanical stress. A simple model suggests that the electric field distortion may be caused by high resistivity contrasts along fault zones and be strongly amplified because of the presence of the resistive crystalline bedrock over a conductive medium. The model also explains the temporal variations of the telluric distortion that are associated with the water level variations in the two lakes separated by the ridge system. The study suggests that the origin of the telluric distortion is the resistivity change in the bedrock resulting from pore pressure change controlled by the lake level variations. The resistivity change in the low-porosity crystalline bedrock is explained in terms of pore connectivity increased as the pressure increases (when the lake levels increase). An important result from this study is that observations made at the laboratory scale have been observed here at the field scale. This paper demonstrates that in environments where there is strong geological heterogeneity and a resistive basement, induced electrical field variations associated with stress can be measured and interpreted quantitatively in terms of subsurface resistivity structure changes.

[31] Whether the model proposed here is relevant for explaining observed electric potential variations associated with earthquakes [*Geller*, 1997] still needs to be investigated. However, it could be one alternative to the often proposed streaming potential effect model [e.g., *Bernard*, 1992]. Currently, there is no satisfactory model that can explain electric potential variations, observed at long distances from earthquakes, in terms of the electrokinetic effect. With a galvanic coupling model, it is possible to estimate the maximum distance from the heterogeneity (origin of the static distortion) over which the off-strike electric field is affected. Indeed, the adjustment distance depends on the size and the dimensionality of the heterogeneity along whose edges charges accumulate [*Menvielle and Tarits*, 1994]. In a 2-D situation, the adjustment distance was shown to be the square root of the integrated conductivity of the upper heterogeneous layer and the integrated resistivity of the resistive layer [*Ranganayaki and Madden*, 1980]. Since on the Sur-Frêtes ridge, the heterogeneity is 2-D at the model scale, the adjustment distance can be reasonably estimated to be about 6 km. The heterogeneity is superficial in the study area (layer thicknesses of 75 and 925 m, though the vertical resolution of the model is smaller than the lateral resolution). Thus, for larger-scale heterogeneity, and in the resistivity situation described here, small resistivity variations could be detected at

long distances (more than tens of kilometers) from fault zones.

Acknowledgments

[32] The author was supported by the European Community through a Marie Curie Fellowship (contract 2001-1669). I am grateful to F. Perrier and P. Tarits for their encouragement and advice. Thanks also to K. Whaler for careful reading of the manuscript, and to P. Glover and two anonymous reviewers for their constructive comments. Contribution 947 of the IUEM, European Institute for Marine Studies (Brest, France).

References

Bahr, K. (1988), Interpretation of the magnetotelluric impedance tensor: Regional induction and local telluric distortion, *J. Geophys.*, *62*, 119–127.

Bahr, K. (2000), Percolation in the crust derived from distortion of electric fields, *Geophys. Res. Lett.*, *27*, 1049–1052.

Bahr, K., M. Smirnov, E. Steveling, and BEAR Working Group (2002), A gelation analogy of crustal formation derived from fractal conductive structures, *J. Geophys. Res.*, *107*(B11), 2314, doi:10.1029/2001JB000506.

Banks, R. (1969), Geomagnetic variations and the electrical conductivity of the upper mantle, *Geophys. J. R. Astron. Soc.*, *17*, 457–487.

Bernard, P. (1992), Plausibility of long distance electrotelluric precursors to earthquakes, *J. Geophys. Res.*, *97*, 17,531–17,546.

Brace, W. F., A. S. Orange, and T. R. Madden (1965), The effect of pressure on the electrical resistivity of water-saturated crystalline rocks, *J. Geophys. Res.*, *70*, 5669–5678.

Chave, A. D., and D. J. Thomson (1989), Some comments on magnetotelluric response function estimation, *J. Geophys. Res.*, *94*, 14,202–14,215.

Chu, J. J., X. Gui, J. Dai, C. Marone, M. W. Spiegelman, L. Seeber, and J. G. Armbruster (1996), Geoelectric signals in China and the earthquake generation process, *J. Geophys. Res.*, *101*, 13,869–13,882.

Counil, J.-L., J.-L. Le Mouël, and M. Menvielle (1986), Associate and conjugate direction concepts in magnetotellurics, *Ann. Geophys.*, *4*, 115–130.

Geller, G. R. (1997), Earthquake prediction: A critical review, *Geophys. J. Int.*, *131*, 425–450.

Glover, P. W. J., J. B. Gómez, and P. G. Meredith (2000), Fracturing in saturated rocks undergoing triaxial deformation using complex electrical measurements: Experimental study, *Earth Planet. Sci. Lett.*, *183*, 201–213.

Groom, R. W., and R. C. Bailey (1989), Decomposition of the magnetotelluric impedance tensor in the presence of local three-dimensional galvanic distortion, *J. Geophys. Res.*, *94*, 1913–1925.

Hautot, S., and P. Tarits (2002), Effective electrical conductivity of 3-D heterogeneous porous media, *Geophys. Res. Lett.*, *29*(14), 1669, doi:10.1029/2002GL014907.

Hautot, S., P. Tarits, F. Perrier, C. Tarits, and M. Trique (2002), Groundwater electromagnetic imaging in complex geological and topographical regions: A case study of a tectonic boundary in the French Alps, *Geophysics*, *67*, 1048–1060.

Jones, A. G. (1988), Static shift of magnetotelluric data and its removal in a sedimentary basin environment, *Geophysics*, *53*, 967–978.

Larsen, J. C. (1975), Low frequency (0.1–6.0 cpd) electromagnetic study of deep mantle electrical conductivity beneath the Hawaiian Islands, *Geophys. J. R. Astron. Soc.*, *43*, 17–46.

Le Mouël, J. L., and M. Menvielle (1982), Geomagnetic variation anomalies and deflection of telluric currents, *Geophys. J. R. Astron. Soc.*, *68*, 575–587.

Madden, T. R., G. A. Latorraca, and S. P. Park (1993), Electrical conductivity variations along the Palmdale segment of the San Andreas fault zone, *J. Geophys. Res.*, *98*, 795–808.

Menvielle, M., and P. Tarits (1994), Adjustment of the electromagnetic field distorted by 3-D heterogeneities, *Geophys. J. Int.*, *116*, 562–570.

Merzer, M., and S. L. Klemperer (1997), Modeling low-frequency magnetic field precursors to the Loma Prieta Earthquake with a precursory increase in fault-zone conductivity, *Pure Appl. Geophys.*, *150*, 27–248.

Miller, S. A., Y. Ben-Zion, and J.-P. Burg (1999), A three-dimensional fluid-controlled earthquake model: Behavior and implications, *J. Geophys. Res.*, *104*, 10,621–10,638.

Muir-Wood, R., and G. C. P. King (1993), Hydrological signatures of earthquake strain, *J. Geophys. Res.*, *98*, 22,035–22,068.

Nolasco, R., P. Tarits, J. H. Filloux, and A. D. Chave (1998), Magnetotelluric imaging of the Society Islands hotspot, *J. Geophys. Res.*, *103*, 30,287–30,309.

Nur, A., and J. R. Booker (1972), Aftershocks caused by fluid flow, *Science*, *175*, 885–887.

Park, S. K., and D. V. Fitterman (1990), Sensitivity of the telluric monitoring array in Parkfield, California, to changes of resistivity, *J. Geophys. Res.*, *95*, 15,557–15,571.

Park, S. K., M. J. S. Johnston, T. R. Madden, F. D. Morgan, and F. F. Morrison (1993), Electromagnetic precursors to earthquakes in the ULF band: A review of observations and mechanisms, *Rev. Geophys.*, *31*, 117–132.

Perrier, F., et al. (1997), A one-year systematic study of electrodes for long period measurements of the electric field in geophysical environments, *J. Geomagn. Geoelectr.*, *49*, 1677–1696.

Perrier, F., M. Trique, B. Lorne, J.-P. Avouac, S. Hautot, and P. Tarits (1998), Electric potential variations associated with yearly lake level variations, *Geophys. Res. Lett.*, *25*, 1955–1958.

Quian, J. (1985), Regional study of the anomalous change in apparent resistivity before the Tangshan earthquake (M 7.8, 1976) in China, *Pure Appl. Geophys.*, *122*, 901–920.

Ranganayaki, R. P., and T. R. Madden (1980), Generalized thin sheet analysis in magnetotellurics: An extension of Price's analysis, *Geophys. J. R. Astron. Soc.*, *60*, 445–457.

Spitzer, K. (1995), A 3D finite difference algorithm for DC resistivity modeling using conjugate gradient methods, *Geophys. J. Int.*, *123*, 903–914.

Spitzer, K. (2001), Magnetotelluric static shift and direct current sensitivity, *Geophys. J. Int.*, *144*, 289–299.

Tarits, P., S. Hautot, and F. Perrier (2004), Water in the mantle: Results from electrical conductivity beneath the French Alps, *Geophys. Res. Lett.*, *31*, L06612, doi:10.1029/2003GL019277.

Tournerie, B., and M. Chouteau (2002), Analysis of magnetotelluric data along the Lithoprobe seismic line 21 in the Blake River Group, Abitibi, Canada, *Earth Planets Space*, *54*, 575–589.

Trique, M., P. Richon, F. Perrier, J.-P. Avouac, and J.-C. Sabroux (1999), Radon emanation and electric potential var-

iations associated with transient deformation near reservoir lakes, *Nature*, *399*, 137–141.

Trique, M., F. Perrier, T. Froidefond, J. Avouac, and S. Hautot (2002), Fluid flow near reservoir lakes inferred from the spatial and temporal analysis of the electric potential, *J. Geophys. Res.*, *107*(B10), 2239, doi:10.1029/2001JB000482.

Walsh, J. B., and W. F. Brace (1984), The effect of pressure on porosity and the transport properties of rock, *J. Geophys. Res.*, *89*, 9425–9431.

White, S. N., A. D. Chave, and J. H. Filloux (1997), A look at galvanic distortion in the Tasman Sea and Juan de Fuca Plate, *J. Geomagn. Geoelectr.*, *49*, 1373–1386.